

Poly(3-hydroxybutyrate-co-3-hydroxyexanoate) Scaffolds with Tunable Macro- and Microstructural Features by Additive Manufacturing

Dario Puppi, Simona Braccini, Antonio Ranaudo and Federica Chiellini*

Department of Chemistry and Industrial Chemistry, University of Pisa, UdR INSTM – Pisa, Pisa, Italy.

* Department of Chemistry and Industrial Chemistry, University of Pisa, UdR INSTM – Pisa, Via G. Moruzzi 13, 56124 Pisa (Italy), e-mail: federica.chiellini@unipi.it

Polymer microstructural engineering by additive manufacturing (AM) represents a powerful tool to functionalize tissue engineering scaffolds. This article reports on the processing of polymer/solvent/non-solvent ternary mixtures through their extrusion in a non-solvent bath as an innovative phase inversion-based AM approach to engineer poly(3-hydroxybutyrate-co-3-hydroxyexanoate) (PHBHHx) scaffolds porosity. The processing of PHBHHx mixtures with different chloroform/ethanol ratio into scaffolds characterized by a dual-scale porosity is described by highlighting how an interconnected network of macropores can be endowed with a tunable microporosity, formed a result of the phase inversion process governing polymer solidification. In particular, the study demonstrates that varying the non-solvent percentage in the ternary mixture represents an effective means to tailor the macropores size along scaffold vertical cross-section and the local micropores concentration in the polymer matrix. These structural changes are demonstrated to significantly affect scaffold overall porosity and tensile modulus, as well as its ability to support *in vitro* the proliferation of preosteoblast cells. The developed manufacturing strategy combines an advanced material engineering method effective on dual-scale size levels, with a modern approach to the sustainable processing of naturally-derived polyesters that minimizes the employment of halogenated solvents.

Keywords: poly(hydroxyalkanoates); poly(3-hydroxybutyrate-co-3-hydroxyexanoate); additive manufacturing, computer-aided wet-spinning, phase separation.

1 Introduction

The introduction of additive manufacturing (AM) into the tissue engineering (TE) field has allowed control enhancement over polymeric scaffolds structure at the macro- and micrometric scale (Mota et al., 2015). Modern AM approaches enable a high degree of automation, good accuracy and reproducibility for the fabrication of clinically-sized, anatomically-shaped scaffolds with tailored composition and a porous architecture characterized by a fully interconnected network of pores with customized size and geometry. Recent advancements on AM of biomedical polymers are resulting in novel materials science and technology tools that are expected to propel the clinical application of TE (Ligon et al., 2017; Janmohammadi and Nourbakhsh 2019). Indeed, anatomical polymeric scaffolds by fused deposition modelling (FDM) were successfully implanted in humans for cranioplasty and oral surgery (Youssef et al., 2017). Ongoing research on combination of AM with other materials processing techniques is focused on endowing scaffolds with microstructural features and optimizing conflicting requirements, such as three-dimensionality and high resolution (Giannitelli et al., 2015). A successful example is represented by computer-aided wet-spinning (CAWS), a hybrid AM approach based on a non-solvent-induced phase separation (NIPS) process governing the coagulation of an extruded polymeric solution which is deposited with a predefined pattern (Puppi et al., 2012). Thus it is possible to obtain a dual-scale porosity integrating a network of macropores with a size determined by the designed lay-down pattern, and a local microporosity in the polymeric matrix formed as a consequence of NIPS process (Mota et al., 2013; Puppi et al., 2016a; Puppi et al., 2016b; Romagnoli et al., 2017; Puppi et al., 2018a). A porosity on dual length scales offers larger pores ensuring efficient nutrients supply and cell migration, together with smaller pores providing high surface area and roughness for cell adhesion and tissue growth (Sommer et al., 2016).

Polyhydroxyalkanoates (PHA) are a class of microbial aliphatic polyesters widely investigated for biomedical applications due to their well-assessed biodegradability and biocompatibility (Morelli et al., 2013; Alves et al., 2016). The wide range of macromolecular structures provided by the numerous PHA homo- and copolymers offers a great versatility in terms of processing and mechanical properties, comparable to that of synthetic aliphatic polyesters (Puppi et al., 2011; Koller 2018). Poly[3-hydroxybutyrate] (PHB) and poly[3-hydroxybutyrate-co-3-hydroxyvalerate] (PHBV) copolymers have been deeply investigated for the engineering of different tissues, such as bone and cartilage (Ke et al., 2017). The longer alkyl side chain confers to poly[3-hydroxybutyrate-co-3-hydroxyhexanoate] (PHBHHx) lower crystallinity and a broader thermal processing window in comparison to PHB and PHBV (Gao et al., 2006). Due to its high elasticity, PHBHHx has been employed for the regeneration of cartilage (Wang et al., 2008), blood vessels (Gao et al., 2019), and tendon (Webb et al., 2013), as well as bone to exploit its piezoelectric behavior and cytocompatibility when cultured with osteoblasts (Wang et al., 2004; Yang et al., 2004; Wang et al., 2005; Jing et al., 2008; Wang et al., 2011; Garcia-Garcia et al., 2012; Ke et al., 2012; Wang et al., 2012; Wu et al., 2013). However, the application of melt-based AM for fabricating PHA scaffolds is limited by their small processing temperatures window (Leroy et al., 2012). A few exceptions are represented by a set of scaffolds based on PHB (Saska et al., 2018) or PHBV (Duan and Wang 2010; Duan et al., 2010; Bin et al., 2011) fabricated by selective laser sintering, as well as PHBV/poly(ϵ -caprolactone) blend scaffolds fabricated by FDM (Kosorn et al., 2016). On the other hand, CAWS was recently shown to be well suited for processing an organic solution of PHBHHx into scaffolds with customized porosity and shape (Mota et al., 2017; Puppi et al., 2017a; Puppi et al., 2018b).

In this context, this study was aimed at the development of a novel CAWS process for the fabrication of PHBHHx scaffolds by processing polymer/solvent/non-solvent ternary

mixtures. CAWS protocols previously reported for PHBHHx processing involve the continuous extrusion of a chloroform solution directly into an ethanol bath (Mota et al., 2017). The processing of ternary mixtures was explored for the first time in this study as an effective means to minimize the employment of chloroform, and tailor scaffold structural features on a dual-scale level by acting on coagulation conditions. CAWS processing of PHBHHx solutions with different chloroform/ethanol ratio (90:10, 80:20, 70:30 or 60:40% v/v) was investigated in order to fabricate scaffolds with predefined shape, dimensions and macroporous architecture. The developed scaffolds were characterized by means of thermogravimetric analysis (TGA), differential scanning calorimetry (DSC), scanning electron microscopy (SEM), uniaxial tensile test under constant strain rate, and in vitro biological evaluation employing MC3T3 murine preosteoblast cells.

2 Materials and Methods

2.1 Materials

Poly(3-hydroxybutyrate-co-3-hydroxyhexanoate) (PHBHHx, 12% mol HHx, $M_w = 300000 \text{ g}\cdot\text{mol}^{-1}$) was kindly supplied by Tsinghua University (Beijing, China). 1,4 dioxane, chloroform and ethanol were purchased from Sigma-Aldrich (Milan, Italy) and used as received without further purification. PHBHHx was purified before use according to the following procedure : (i) the polymer was dissolved in 1,4 dioxane (5% w/v) under stirring for 1 h at room temperature; (ii) the obtained solution was centrifuged at 4000 rpm for 1 h; (iii) the supernatant was slowly dropped into 10-fold volume water; (iv) the precipitated polymer was collected by filtering; (v) the polymer was washed with distilled water and then ethanol, vacuum dried and stored in a desiccator.

2.2 *Polymeric Mixtures Preparation*

PHBHHx solutions in chloroform were prepared by adding 1.25 g of the polymer to 5 ml of the solvent and the obtained mixtures were left at 30 °C under magnetic stirring for 3 h until complete polymer dissolution. Ternary polymer/solvent/non-solvent mixtures with different chloroform/ethanol volumetric ratio (90:10, 80:20, 70:30, 60:40 and 50:50 % v/v) were prepared by employing two different methods (**Table 1**).

[Table 1 near here]

Method 1 (M1): i) 1.25 g of polymer was dissolved in a given volume of chloroform under magnetic stirring at 30 °C for 2 h; ii) ethanol was added dropwise to the polymer solution to reach a total solvent/non-solvent volume of 5 ml, and the obtained mixture was left under stirring at room temperature for 1 h.

Method 2 (M2): i) chloroform and ethanol were mixed under magnetic stirring at a given volumetric ratio to obtain a total volume of 5 ml; ii) 1.25 g of polymer was added to the solvent/non-solvent mixture and the obtained ternary system was left under magnetic stirring at 30 °C for 3 h.

2.3 *Scaffolds Fabrication*

Scaffolds were fabricated by means of a CAWS system enabling the simultaneous control of the feed rate of a polymeric solution and its lay-down pattern, as described elsewhere (Mota et al., 2017). The desired polymeric mixture was placed into a glass syringe fitted with a metallic needle (inner diameter 0.4 mm, Gauge 22) and then injected at a controlled feeding rate directly into an ethanol bath by using a programmable syringe pump. The coagulating polymeric solution was deposited with a predefined lay-down pattern through the computer-controlled synchronized motion of the needle and the deposition platform (**Figure 1a**). The

3D geometrical scaffold parameters were designed by using an algorithm developed in Matlab software (The Mathworks, Inc., Natick, MA, USA): 0–90° lay-down pattern (α), theoretical distance between fibers axes (d_{XY}) of 200 μm and inter-layer needle translation (d_z) of 80 μm (**Figure 1b**). Samples with a designed base size of 12x12 mm² and composed by different number of layers (16 or 40) were fabricated. After fabrication, the sample was removed from the coagulation bath, left under a fume hood for 24 h, placed in a vacuum chamber at 0.5 mbar for 8 h and then stored in a desiccator for at least 48 h before characterization.

[Figure 1 near here]

2.4 Morphological Characterization

The top-view and perpendicular cross-section (obtained by fracture in liquid nitrogen) of the scaffolds were analyzed by means of field emission scanning electron microscopy (FE-SEM, Quanta-FEG 450, Thermo Fisher Scientific, Waltham, MA, USA) at CISIM research center for Materials Science and Engineering, University of Pisa, Italy. The scaffold morphological parameters were measured on SEM micrographs by means of ImageJ 1.43u software (National Institutes of Health, Bethesda, MD, USA). The average fiber diameter and macropores size in the XY plane were measured on top-view micrographs, while the macropores size along the Z axis was measured on perpendicular cross-section micrographs (50X magnification, data calculated over 20 measurements per scaffold). Micropores size and concentration were measured on top-view micrographs (2000X magnification, data calculated over 50 measurements per scaffold). Micropores concentration was determined by counting the number of pores within a 500 μm^2 square and expressed as number of pores per mm².

2.5 Thermal Analysis

Scaffolds' thermal properties were evaluated by means of thermogravimetric analysis (TGA) and differential scanning calorimetry (DSC) on three replicates for each kind of sample. TGA was performed using a TGA Q500 instrument (TA Instruments, Milan, Italy) in the temperature range 30–400 °C, at a heating rate of 10 °C·min⁻¹ and under a nitrogen flow of 60 mL·min⁻¹. The samples' thermal decomposition was evaluated by analyzing the weight and derivative weight profiles as function of temperature. The degradation temperature (T_{deg}) was determined as the temperature corresponding to a percentage weight loss of 0.5 %. DSC analysis was carried out using a Mettler DSC-822 instrument (Mettler Toledo, Milan, Italy) through two heating cycles in the range –25 to 180°C under a nitrogen flow rate of 80 mL·min⁻¹, at a heating rate of 10 °C·min⁻¹ and a cooling rate of 20 °C·min⁻¹. By analyzing the first heating cycle, the melting temperature (T_m) was considered as the second endothermic peak temperature and the crystallinity degree (Cr) was calculated by analyzing the area of the three endothermic peaks and considering a melting enthalpy of 100 per cent crystalline PHB of 146.6 J·g⁻¹ (Yang et al., 2009). The glass transition temperature (T_g) was obtained by analyzing the curve inflection point in the first and second heating cycle.

2.6 Porosity Calculation

The overall porosity of the scaffolds was estimated by means of the following equation (Li et al., 2008):

$$P = \frac{D_p - D_s}{D_p} \quad Eq. 1$$

where DS is the density of the scaffold defined as the ratio between its weight and its total volume calculated from its actual dimensions taken with a digital caliper, and DP is the structural density of the polymeric phase calculated by applying the following equation:

$$D_p = \frac{1}{\frac{1 - Cr}{D_a} + \frac{Cr}{D_c}} \quad Eq. 2$$

where D_a is the density of PHBHHX amorphous domains ($1.18 \text{ g}\cdot\text{mL}^{-1}$), D_c is the density of PHBHHx crystalline domains ($1.26 \text{ g}\cdot\text{mL}^{-1}$) and Cr is the crystallinity degree obtained from DSC analysis.

2.7 Mechanical Testing

Tensile mechanical properties of the PHBHHx scaffolds were evaluated under a constant strain rate in phosphate buffered saline 1X (PBS) at 37°C , using a dynamic mechanical thermal analyzer (DMTA-V, Rheometric Scientific, Germany). A total of five samples of each kind of scaffold with a width of $4.35 \pm 0.35 \text{ mm}$ and a thickness of $1.00 \pm 0.15 \text{ mm}$ (16 layers) were tested by setting a gauge length of 7.50 mm . The specimens were left at 37°C in PBS for 2 h prior testing and then fixed to tensile clamps (torque of 20 cNm). The tensile test was carried out at 37°C in PBS by applying a strain rate of $3.5 \text{ mm}\cdot\text{min}^{-1}$ parallel to the axes of the longitudinal fibers of the sample (ASTM 2010; Puppi et al., 2018b). The stress (σ) was defined as the ratio between the measured force and the original cross-section area of the sample calculated from its actual dimensions measured by means of a digital caliper, while the strain (ϵ) as the ratio between the sample height variation and its initial height. In the stress-strain curves, the tensile modulus was calculated as the slope of the initial roughly linear region, and the stress and strain at break were considered as the relevant values at the sample breaking point.

2.8 Biological Characterization

Preliminary biological evaluation of selected scaffolds was performed employing the mouse calvaria-derived pre-osteoblastic cell line MC3T3-E1 obtained from American Type Culture

Collection (ATCC CRL 2594). Cells were propagated as indicated by the supplier using Minimum Essential Medium Eagle alpha modification (α -MEM) (Sigma), containing ribonucleosides, deoxyribonucleosides, sodium bicarbonate and supplemented with 2 mM of L-glutamine (Sigma), 1 % of penicillin:streptomycin solution (10,000 U/ml:10 mg·ml⁻¹)(Sigma), 10% of fetal bovine serum(FBS) (Sigma) and antimycotic (InvivoGen). The cultures were maintained at 37 °C and in a 5% CO₂-enriched atmosphere.

2.8.1 Cell Seeding

Scaffold samples were placed in a 24 wells plate, sterilized under UV light for 20 minutes on each side and then washed with 70 % ethanol:water solution for 1 hour. After ethanol removal, scaffolds were extensively washed with Dulbecco's phosphate buffer saline (DPBS)(Sigma), containing a penicillin/streptomycin solution (1 %). The solution was then substituted with complete culture medium and samples were incubated at 37 °C and in a 5% CO₂-enriched atmosphere for 48 hours before cell seeding. Subsequently 3 x 10⁴ cells were seeded onto scaffold in a 24 well plate and, after 30 minutes of incubation at 37 °C and 5 % CO₂, 700 μ l of complete medium were added to each well, followed by incubation in a humidified atmosphere at 37 °C.

2.8.2 Cell Viability and Proliferation

Cell viability and proliferation were measured by using the cell proliferation reagent WST-1 (Roche Applied Science, Indianapolis, IN, USA) at 7 and 16 days of cell culture. The test is based on the mitochondrial enzymatic conversion of the tetrazolium salt WST-1 into formazan, the soluble product. Briefly, cell-seeded scaffolds were incubated for 4 hours with the WST-1 reagent, diluted 1:10, at 37 °C and 5 % CO₂. Measurements of formazan dye absorbance were carried out with a microplate reader (Biorad, Milan, Italy) at 450 nm, with the reference wavelength at 655 nm.

2.8.3 Cell Morphology Investigation by Confocal Laser Scanning Microscopy (CLSM)

Morphology of MC3T3-E1 cells grown on the prepared scaffolds and 3D culture organization were investigated by means of CLSM at days 7 and 16 after seeding. Cells cultured on scaffold were fixed with 3.8% p-formaldehyde for 1 hour in PBS 1X, permeabilized with a PBS 1X/Triton X-100 solution (0.2 % v/v) (Sigma) for 10 min, blocked with bovine serum albumin (BSA, 0.1% w/v in PBS 1X) (Sigma) for 30 minutes. Samples were then incubated with a solution of phalloidin-Alexa Fluor 488 (Invitrogen) for 1 hour and with 4'-6-diamidino-2-phenylindole (DAPI) (Invitrogen) for 30 minutes at room temperature in the dark. After dye incubation, samples were washed three times with PBS and observed under a Nikon Eclipse TE2000 inverted microscope equipped with an EZ-C1 confocal laser and Differential Interference Contrast (DIC) apparatus (Nikon, Japan). A 405 nm laser diode and an Argon Ion Laser (488 nm emission) were used to excite respectively DAPI and phalloidin fluorophores. Images were captured with Nikon EZ-C1 software with identical instrumental settings for each sample. Images were further processed and merged with Adobe Photoshop CC (Creative Cloud) 2015 software.

2.9 Statistical Analysis

Experimental data were reported as mean \pm standard deviation. Statistical differences were analyzed using one-way analysis of variance (ANOVA), and a Tukey test was used for post hoc analysis. A p value < 0.05 was considered statistically significant.

3 Results and Discussion

3.1 Scaffolds Fabrication

The solubility of PHBHHx in mixtures with different solvent/non-solvent ratio (90:10, 80:20,

70:30, 60:40 and 50:50 % v/v) was investigated in order to develop a CAWS fabrication process involving the processing of ternary solutions. On the basis of previous studies on PHBHHx processing by CAWS (Mota et al., 2017; Puppi et al., 2018b), chloroform was selected as solvent, ethanol as non-solvent, and 25% w/v as optimized polymer concentration. Polymer solubility in ternary mixtures was investigated by following the two previously described experimental methods: the first one involving the solubilization of PHBHHx in chloroform and then the addition of ethanol to the polymer solution (M1); the second one involving the direct solubilization of PHBHHx in a chloroform/ethanol mixture (M2). As summarized in **Table 1**, the polymer was completely soluble in 90:10, 80:20 and 70:30% v/v solvent/non-solvent mixtures. The presence of small insolubilized particles suspended in 60:40% v/v mixtures indicated that the polymer solubility limit was reached, though the resulting ternary mixtures could be processed to fabricate PHBHHx scaffolds, as described later. Polymer precipitation was observed in 50:50% v/v mixtures making them not suitable for a reproducible fabrication process. In all cases, the mixing method employed did not influence the resulting polymer solubility.

The CAWS fabrication process involved the extrusion of the desired polymeric mixture through a needle that was immersed into an ethanol bath to build up a 3D porous scaffold with a layer-by-layer process based on a 0-90° lay-down pattern (**Figure 1**). PHBHHx scaffold prototypes with $d_{XY} = 0.2$ mm and different number of layers (16 or 40 layers) were successfully fabricated by processing 90:10, 80:20, 70:30 and 60:40% v/v polymeric mixtures (**Figure 2**). The optimized processing parameters applied to all mixtures were deposition velocity ($V_{dep} = 600 \text{ mm} \cdot \text{min}^{-1}$), initial distance between the tip of the needle and the deposition surface ($Z_0 = 2$ mm), inter-layer Z needle translation ($dz = 0.08$ mm), and solution feed rate ($F = 0.3 \text{ ml} \cdot \text{h}^{-1}$). From a macroscopical point of view, scaffolds fabricated

by employing different mixtures did not show any marked difference in terms of fibers alignment, pores geometry, and external shape.

[Figure 2 near here]

PHA synthesized in bacteria are considered environmentally friendly and sustainable materials that can be used to partially replace petroleum-based plastics (Wang and Chen 2017). Great efforts have therefore been made to reduce the cost production of PHA and enhance the competitiveness of their large-scale commercialization through new technologies via metabolic engineering, synthetic biology, and bioinformatics (Koller et al., 2017). Halogenated solvents, in particular chloroform and dichloromethane, are considered as election solvents for PHA extraction and processing because of their high solubilizing properties. In general, PHA solubility is achieved when hydrocarbons carrying at least one chlorine atom and one hydrogen atom are employed as solvents (Jacquel et al., 2007). This is the result of a polar interaction between the chloride atom and the carbon that holds the carbonyl function, and a linking between the hydrogen atom of the halogenated compound and the carbonyl function of the polymer. Health risks that halogenated solvents pose to mankind and relevant environmental concerns have encouraged research on employment of non-halogenated solvents for PHA extraction and processing (Kourmentza et al., 2017). In general, the minimization of the use of toxic organic solvents from manufacturing methods is widely investigated with the aim of broadening the range of applications and improve the safety of medical and pharmaceutical products.

To mitigate the toxicities of toxic organic solvent-based manufacture methods, we have designed a method for the formulation of PTX nanosuspensions (PTX-PEG [polyethylene glycol]-HSA [human serum albumin]) that eliminates the dependence on toxic organic solvents.

The present study significantly contributes to this research trend by offering a novel protocol for PHBHHx scaffolds production involving the replacement of up to 40% v/v of chloroform with ethanol, which is classified by the European Medicine Agency as solvent with low toxic potential and allowed as residue in medical products.

3.2 *Thermal Analysis*

TGA and DSC analysis of the developed scaffolds were carried out to evaluate the influence of the starting mixture composition and the method employed for its preparation on the resulting material thermal and structural properties.

TGA analysis showed that all the samples shared a similar thermal degradation profile with a degradation temperature (T_{deg}) in the range 220–250 °C. A peak centered at around 285 °C was evident in all thermal degradation derivative curves (**Figure 3a**). The peculiar single weight-loss degradation of short chain PHA is the result of a complex decomposition mechanism beginning with chain scission of the ester linkages and the formation of unsaturated carboxyl acids and unsaturated esters (Kopinke et al., 1996; Li et al., 2003; Xiang et al., 2016).

[Figure 3 near here]

TGA data comparison showed that PHBHHx scaffolds had a significantly higher T_{deg} in comparison to raw polymer (**Table 2**). In agreement with previous studies on wet-spinning of PHBHHx (Puppi et al., 2018b), this result might be due to a purification effect during polymer coagulation in ethanol leading to the removal of impurities with a lower T_{deg} in comparison to PHBHHx. No remarkable differences in thermal degradation profile nor significant differences in T_{deg} were detected between scaffolds fabricated by employing different solvent/non-solvent ratios and different mixing methods.

[Table 2 near here]

The first heating DSC curves of the analyzed samples were characterized by a glass transition at around 0 °C and a multi-step endothermic profile (**Figure 3b**). In particular a first endotherm (I) centered at around 55 °C, a second one (II) centered in the range 85-95 °C, and a third one (III) centered at around 105 °C were detected. The three endothermic peaks can be related to the melting of different lamellar crystalline domains formed during polymer solidification (Sato et al., 2004; Yang et al., 2009; Ding et al., 2011). In particular, endotherm II is likely due to the melting of primary lamellae and endotherm I to the melting of secondary lamellae, while endotherm III to the melting of lamellae formed through reorganization or thickening of primary and/or secondary lamellae upon heating (Ding et al., 2011). The melting temperature (T_m) was taken as the temperature corresponding to the minimum of endotherm II, and the crystallinity degree (Cr) was calculated from the area of the three peaks (**Table 2**).

Overall, DSC scaffolds thermograms were characterized by a sharper and higher second peak which was shifted to significantly higher T_m , as well as a less pronounced third peak in comparison to that of raw polymer (Puppi et al., 2017b; Puppi et al., 2018b). As a consequence, Cr of scaffolds was significantly higher than that of the raw polymer. These differences can be related to a more uniform thickness distribution of crystalline lamellae in scaffolds (Ding et al., 2011), as a result of the different solidification processes involved, i.e., dropping in water as final step of material purification in the case of raw polymer, and coagulation in ethanol in the case of wet-extrusion during scaffold fabrication. Differences in T_m and Cr between scaffolds fabricated by employing mixtures with different composition and/or prepared by means of different mixing methods were not statistically significant.

A more pronounced glass transition and no melting peaks were detected in the second heating curves of all samples due to the relatively rapid cooling from melt (20 °C·min⁻¹) that

did not allow the formation of crystalline domains (Lim et al., 2006). No significant differences in T_g were observed between different samples both in the first and second heating scans, suggesting that material processing and variation of solvent/non-solvent ratio did not cause remarkable chemical-physical changes in the macromolecular structure of PHBHHx.

3.3 *Morphological Analysis*

SEM image analysis was carried out to assess the influence of polymeric mixture composition and its preparation method on the morphology of the resulting 3D scaffolds. The morphological investigation highlighted a good reproducibility of the internal architecture and a good degree of fibers alignment for all PHBHHx scaffolds developed. Top view and perpendicular cross-section micrographs analysis highlighted that the scaffolds were composed by overlapped layers of aligned fibers forming a network of macropores fully interconnected along the three dimensions (**Figure 4**). Marked differences in the layered structure detectable by comparing perpendicular cross-section micrographs of different samples were mainly due to polymer plastic deformation during fracture in nitrogen. Indeed, although the samples were left in nitrogen for a few minutes before their fracture, the relatively low T_g of the polymer often did not allow to achieve a totally brittle fracture. Partial plastic deformation of the polymer matrix was also observed in high magnification micrographs of the single fibers cross-section (**Figure 5**). In addition, both the outer surface and cross-section of the fibers constituting the scaffolds were characterized by a microporous morphology. Such microporosity is formed as a consequence of the phase inversion process behind polymer coagulation and solidification during extrusion in a non-solvent. Indeed, the solvent/non-solvent counter diffusion in and out the coagulating filament leads to a thermodynamic instability in the polymeric solution that separates into two phases with

different composition. Under critical coagulation parameters, a polymer-lean phase is dispersed in a continuous polymer-rich phase leading to the formation of a microporous matrix after polymer solidification and solvent/non-solvent removal (Biazar et al., 2016; Puppi and Chiellini 2017). The resulting dual-scale porous architecture integrating a macroporous network determined by the computer-controlled lay-down pattern and a phase inversion-induced microporosity is a peculiar structural feature of polymeric scaffolds fabricated by CAWS, representing a powerful tool to tailor fundamental scaffold properties strongly dependent on its porosity (Puppi and Chiellini 2017).

[Figures 4 and 5 near here]

A quantitative evaluation of the effect of solvent/non-solvent ratio in the mixture on scaffold macro- and microstructural features was carried out by measuring morphological parameters on different size scales, such as fiber diameter, macropores size along Z axis, micropores concentration and overall porosity (**Figure 6**).

[Figure 6 near here]

It is worthy to note that, besides melt electrospinning writing that enables the obtainment of submicrometric fibers (Puppi and Chiellini 2018), the described AM process has higher resolution in comparison to FDM that typically result in scaffolds with filament diameters in the range of 100–500 μm . Indeed, mean fiber diameter of the developed scaffolds falls in the range 50–80 μm . M-100S scaffolds were characterized by a significantly smaller fiber size ($57.8 \pm 7.9 \mu\text{m}$) in comparison to scaffolds fabricated from ternary mixtures whose mean fiber sizes were in the range 66–78 μm . In addition, scaffolds fabricated by processing 60:40 and 70:30% v/v mixtures, as well as M1-80S-20NS scaffolds, showed a significantly larger fiber size when compared to other types of scaffold. As evident from perpendicular cross-section SEM micrographs (**Figure 4 and 5**), scaffolds from 60:40% v/v

solvent/non-solvent mixtures were characterized by two populations of fibers with significantly different size. In particular, M1-60S-40NS scaffolds had a fiber population with a size of $78.6 \pm 5.2 \mu\text{m}$ and another one with a size of $62.2 \pm 4.1 \mu\text{m}$, while M2-60S-40NS scaffolds had two fiber populations with size of 86.2 ± 4.1 and $60.0 \pm 2.3 \mu\text{m}$.

The mean values of XY pores size were in the range 104-117 μm with no significant differences between different kinds of scaffolds, due to the relatively large standard deviation. However, by varying the non-solvent percentage in the ternary mixture, significant variations in terms of Z axis pore size, micropores concentration and overall porosity were observed. In particular, scaffolds from ternary mixtures had a Z axis pore size significantly larger than the reference M-100S scaffold. In addition, scaffolds from 60:40 mixtures had Z pore mean size of around 70 μm , significantly larger than the other kinds of scaffolds.

The micropores observed in the high magnification micrographs of the polymeric matrix had a mean size value in the range 1-3 μm with no significant differences between scaffolds fabricated by varying chloroform/ethanol ratio. However, by increasing the non-solvent percentage in the polymeric solution, a significantly growing concentration of micropores in the range 5-80 pores per mm^2 was detected. Overall, the differences observed through morphological analysis resulted in a trend of total porosity growing in the range 70-90% by increasing non-solvent percentage in the ternary mixture.

The presence of a non-solvent in the starting polymeric solution and the variation of its percentage could have affected the thermodynamic and kinetic conditions of the phase inversion process leading to the variations in scaffold macro e microstructural properties summarized in **Figure 6**. Indeed, as previously described, NIPS is the result of solvent/non-solvent counter-diffusion until the solution becomes thermodynamically unstable and demixing takes place, leading to the formation of a solid polymeric fiber. According to the theory behind NIPS and the experimental evidence from studies on membranes and fibers

formation through non-solvent dipping (Wang et al., 1995; Barton et al., 1997; Wang et al., 2002), the addition of a non-solvent to a polymer solution can influence polymer solvation as well as the miscibility between the ternary mixture and the coagulation bath, with the overall result of affecting the demixing kinetics. The increasing Z pores size between different scaffolds is likely related to a faster coagulation leading to less pronounced fiber flattening at the contact points as observed in SEM micrographs (**Figures 4 and 5**).

The demonstrated effect on fiber micropores concentration corroborates the findings of a large body of literature showing the possibility of tuning surface microporosity by adding a non-solvent to a polymeric solution that is then submitted to NIPS (Guillen et al., 2011). Indeed, non-solvent additives are employed to suppress macrovoids formation and obtain a porous skin layer in membranes and fibers by NIPS (Lin et al., 2002). The peculiar dual-size fibers population previously described for scaffolds from 60:40% v/v mixtures is likely related to the aforementioned faster solidification. Indeed, coagulation rate can have a marked influence on variations in fiber stretching as consequences of needle acceleration/deceleration before and after changes in deposition direction.

3.4 Mechanical Characterization

The influence of polymeric mixture composition and preparation method on the mechanical properties of the resulting scaffolds was investigated under a constant tensile strain rate in PBS at 37 °C. Stress-strain curves of representative PHBHHx samples are reported in **Figure 7a**. Overall, the curves were characterized by an initial linear region with a mean value of the tensile modulus in the range 2.4-5.2 MPa, then a transition to a region characterized by a gradual decrease of the stress on increasing the strain up to sample break at a strain in the range 15-45%. The longitudinally aligned fibers were those mainly involved in load bearing, being stretched along their axis before break resulting in sample failure (Puppi et al., 2018b).

[Figure 7 near here]

M-100-S scaffolds showed significantly higher tensile modulus and stress at break than the other samples (**Figures 7b and 7C**). On the contrary, scaffolds fabricated by processing 60:40% v/v mixtures showed significantly lower tensile modulus and stress at break than the other scaffolds. A comparative analysis of morphological and mechanical parameters (**Figures 6 and 7**) suggests that Z axis pore size and fiber fusion at the layer-layer contact points are the most influent parameters affecting scaffolds mechanical parameters. Indeed, Z axis pore size varied from 33 to 75 μm by increasing non-solvent percentage in the ternary mixture, resulting in porosity change from 75 to 86% with corresponding variations of tensile modulus from 5.2 to 2.4 MPa and stress at break from 0.31 to 0.18 MPa. In addition, the reduced fibers flattening and fusion at the contact points observed in scaffolds fabricated by employing a 60:40% v/v solvent/non-solvent ratio (**Figure 5**) resulted in a more marked sample delamination during the tensile test, which explains the drop in relevant mechanical parameters.

The development of polymeric scaffolds tailored to TE applications should take into account different structural and mechanical requirements (Bose et al., 2012). Indeed, the scaffold should preserve its shape, size and porous structure while handled during sterilization, packing, transportation, possible *in vitro* cell culture, and surgery. Once implanted, the tissue engineered construct should withstand the physiological stresses and transfer them without shielding effects, and at the same time, it should maintain an interconnected porous structure for optimal tissue ingrowth and mechanical interlocking with the hosting tissues. For instance, in the case of bone engineering a pore size larger than 100 μm and an overall porosity exceeding 70% is usually required to achieve effective osteogenesis (Karageorgiou and Kaplan 2005). Considering that the stiffness and strength of the scaffold decrease by increasing the void volume, the porous architecture should be finely

tuned to assure contemporarily the development of an integrated tissue within scaffold pores and the structural role of the implant. This design aspect is critical in the case of scaffolds endowed with a dual-scale porous structure like in the case of those fabricated by CAWS. Indeed, the microporosity of the polymeric matrix on one side can be exploited to tune key material properties (e.g., biodegradation rate, material/cell interaction and release of loaded drugs) and on the other can lead to decreased material stiffness (Choren et al., 2013). In this optic, the strategy proposed by the reported study based on ternary mixture composition/scaffold porosity relationship provides a powerful tool to finely tune fundamental scaffold structural and mechanical properties.

Concerns about the relatively low stiffness of this kind of polymeric scaffolds in comparison to bone tissues that typically experience high stresses and low strains in physiological conditions are often raised. However, dual-scale porous polymeric constructs with mechanical properties comparable to those found in this study possessed the structural stability required for *in vivo* regeneration of non-load-bearing bone tissue (Dini et al., 2016). In addition, it should be considered that scaffold elasticity influences cell shape, cytoskeletal organization, function, protein expression, and differentiation (Engler et al., 2006). Bone formation and mineralization *in vivo* starts in the osteoid, i.e., a crosslinked collagen matrix with an elastic modulus of 20-50 kPa (Iismaa et al., 2018), which is even lower than that of PHBHHx. Scaffolds with stiffness in this order of magnitude have been found optimal to provide *in vivo* 3D environments for enhanced osteogenic differentiation, cell recruitment, and angiogenesis (Chen et al., 2015).

3.5 Biological Characterization

Investigation of MC3T3-E1 preosteoblast cell line proliferation onto the developed scaffolds was performed using the WST-1 tetrazolium salt assay at day 7 and 16 of culture. Results are

depicted in **Figure 8**.

[Figure 8 near here]

At day 7 of culture, the limited cell proliferation observed for all the typologies of scaffolds could be related to the large pore size and thin fibers diameter of the scaffolds that did not facilitate the retention of a significant number of the cells during the seeding procedure. However, despite the poor initial cell adhesion and proliferation, a significant increase in scaffold cellular colonization was observed for all the tested samples at day 16 of culture. Results highlighted significant differences in cell proliferation on the various types of sample, that could be correlated to the differences in micropores concentration exhibited by the analyzed scaffolds as reported in **Figure 6** (Zhang et al., 2018). In particular, samples M-100S and M2-90S-10NS that are characterized by the lowest micropores concentration, appear less suited for an optimal cell colonization. All the remaining scaffolds, that display a significantly higher micropores concentration, resulted better suited for a sustained cell proliferation.

The increasing trend in cell proliferation correlated to the micropores concentration however is not observed in the case of sample M1-60S-40NS, which even if characterized by the highest concentration of micropores, showed a decrease in cell proliferation. These results can be attributed to the large size of the macropore along the z axis exhibited by the scaffold, that could hinder optimal colonization of the scaffolds and in particular the inter-fibers bridging.

CLSM, employed to observe cell morphology and distribution onto the investigated scaffolds by means of fluorescent staining of cytoskeleton (phalloidin-Alexa Fluor 488) and nuclei (DAPI), confirmed the quantitative results. At 16 days of cell culture, microscopic observation showed a good surface colonization of the scaffolds by MC3T3-E1 cells and the beginning of the formation of inter-fiber junction bridges in M1-70S-30NS and M2-70S-

30NS scaffolds (**Figure 9**). Moreover, the cellular architecture showed the organization of F-actin comparable to that typical of the early stages of cellular adaptation to the material (Hutmacher et al., 2001), exhibiting great stress fibers stretched along the cytoplasm and suggesting a good adhesion to polymer substrates.

[Figure 9 near here]

4 Conclusion

This study has shown that PHBHHx scaffolds with predefined shape, size and porous architecture can be additively manufactured by processing ternary polymer/chloroform/ethanol mixtures with different composition. This innovative approach represents a suitable means to enhance the environmental sustainability of CAWS process for PHBHHx scaffolds production by replacing with ethanol up to 40% v/v of the chloroform employed. In addition, the evidence that the variation of the non-solvent percentage in the ternary mixture has a significant effect on scaffold structural features at hierarchical macro- and microstructural levels provides a powerful tool to tailor key scaffold properties without acting on material composition or other fabrication parameters. Such dual-scale porosity can mimic the intrinsic hierarchical structure of natural bone consisting of larger osteons (~100 μm diameter) and vascular channels, as well as smaller lacuna spaces (~10 μm diameter) (Currey 2012). Its tuning, besides affecting mechanical properties and cell proliferation as shown by this study, can be exploited to optimize other fundamental properties strictly related to scaffold porosity, such as biodegradation rate, release of bioactive agents possibly loaded in the polymer matrix, and tissue-stimulating piezoelectric effect (Puppi and Chiellini 2017). Investigations in this context will pave the way for advanced materials engineering strategies tailored to the bioactive functionalization of additive manufactured scaffolds.

Future work will address the fabrication of PHBHHx scaffolds from ternary mixtures without the use of a coagulation bath by means of a phase inversion process based on the controlled evaporation of the solvent/non-solvent system. Indeed, NIPS can be induced in a ternary mixture through a controlled variation of its composition, achieved by means of the contemporary evaporation at a given temperature of a more volatile solvent and a less volatile non-solvent (Wijmans and Smolders 1982). This approach will be explored in order to minimize the overall employment of organic solvents with the goal of optimizing advanced materials technology strategies for the low-environmental impact fabrication of scaffolds based on naturally-derived polyesters.

Acknowledgements

The financial support of the University of Pisa PRA-2016-50 and PRA-2018-23 projects entitled “Functional Materials” and the Tuscany Region (Italy) funded Project “Nuovi Supporti Bioattivi a Matrice Polimerica per la Rigenerazione Ossea in Applicazioni Odontoiatriche (R.E.O.S.S.)” as part of the program POR CREO FESR 2007–2013—Le ali alle tue idee are gratefully acknowledged. PHBHHx was kindly supplied by Guo-Qiang Chen of Tsinghua University (Beijing, China) within the framework of the EC-Funded project Hyanji Scaffold in the People Program of the 7FP (2010–2013). Dr. Randa Ishak is acknowledged for her support in recording SEM images.

Declaration of interest statement

No potential conflict of interest was reported by the authors.

References

- V.D. Alves, C.A.V. Torres and F. Freitas **Bacterial polymers as materials for the development of micro/nanoparticles**. *Int. J. Polym. Mater. Polym. Biomater.*, 65 (2016), pp. 211-224.
- ASTM D882 Tensile Properties of Thin Plastic Sheeting (2010)
- B.F. Barton, J.L. Reeve and A.J. McHugh **Observations on the dynamics of nonsolvent-induced phase inversion**. *J. Polym. Sci., Part B: Polym. Phys.*, 35 (1997), pp. 569-585.
- E. Biazar, D. Momenzadeh, S.H. Keshel, F. Yousefi, M. Shabaniyan, F. Sefidabi and M. Sheikholeslami **Solvent effect in phase separation for fabrication of micropatterned**

porous scaffold sheets. *Int. J. Polym. Mater. Polym. Biomater.*, 65 (2016), pp. 351-357.

D. Bin, C. Wai Lam and W. Min **Optimized fabrication of Ca–P/PHBV nanocomposite scaffolds via selective laser sintering for bone tissue engineering.** *Biofabrication*, 3 (2011), pp. 015001.

S. Bose, M. Roy and A. Bandyopadhyay **Recent advances in bone tissue engineering scaffolds.** *Trends Biotechnol.*, 30 (2012), pp. 546-554.

G. Chen, C. Dong, L. Yang and Y. Lv **3D Scaffolds with Different Stiffness but the Same Microstructure for Bone Tissue Engineering.** *ACS Appl. Mater. Interfaces*, 7 (2015), pp. 15790-15802.

J.A. Choren, S.M. Heinrich and M.B. Silver-Thorn **Young's modulus and volume porosity relationships for additive manufacturing applications.** *J. Mater. Sci.*, 48 (2013), pp. 5103-5112.

J.D. Currey **The structure and mechanics of bone.** *J. Mater. Sci.*, 47 (2012), pp. 41-54.

C. Ding, B. Cheng and Q. Wu **DSC analysis of isothermally melt-crystallized bacterial poly(3-hydroxybutyrate-co-3-hydroxyhexanoate) films.** *J. Therm. Anal. Calorim.*, 103 (2011), pp. 1001-1006.

F. Dini, G. Barsotti, D. Puppi, A. Coli, A. Briganti, E. Giannessi, V. Miragliotta, C. Mota, A. Piroso, M.R. Stornelli, P. Gabellieri, F. Carlucci and F. Chiellini **Tailored star poly(ϵ -caprolactone) wet-spun scaffolds for in vivo regeneration of long bone critical size defects.** *J. Bioact. Compat. Polym.*, 31 (2016), pp. 15-30.

B. Duan and M. Wang **Customized Ca–P/PHBV nanocomposite scaffolds for bone tissue engineering: design, fabrication, surface modification and sustained release of growth factor.** *J. R. Soc. Interface*, 7 (2010), pp. S615-S629.

B. Duan, M. Wang, W.Y. Zhou, W.L. Cheung, Z.Y. Li and W.W. Lu **Three-dimensional nanocomposite scaffolds fabricated via selective laser sintering for bone tissue engineering.** *Acta Biomater.*, 6 (2010), pp. 4495-4505.

A.J. Engler, S. Sen, H.L. Sweeney and D.E. Discher **Matrix Elasticity Directs Stem Cell Lineage Specification.** *Cell*, 126 (2006), pp. 677-689.

J. Gao, H. Guo, S. Tian, Y. Qiao, J. Han, Y. Li and L. Wang **Preparation and mechanical performance of small-diameter PHBHHx vascular graft by electrospinning.** *Int. J. Polym. Mater. Polym. Biomater.*, 68 (2019), pp. 575-581.

Y. Gao, L. Kong, L. Zhang, Y. Gong, G. Chen, N. Zhao and X. Zhang **Improvement of mechanical properties of poly(dl-lactide) films by blending of poly(3-hydroxybutyrate-co-3-hydroxyhexanoate).** *Eur. Polym. J.*, 42 (2006), pp. 764-775.

J.M. Garcia-Garcia, L. Garrido, I. Quijada-Garrido, J. Kaschta, D.W. Schubert and A.R. Boccaccini **Novel poly(hydroxyalkanoates)-based composites containing Bioglass (R) and calcium sulfate for bone tissue engineering.** *Biomed. Mater.*, 7 (2012), pp. 054105.

S.M. Giannitelli, P. Mozetic, M. Trombetta and A. Rainer **Combined additive manufacturing approaches in tissue engineering.** *Acta Biomater.*, 24 (2015), pp. 1-11.

G.R. Guillen, Y. Pan, M. Li and E.M.V. Hoek **Preparation and Characterization of Membranes Formed by Nonsolvent Induced Phase Separation: A Review.** *Ind. Eng. Chem. Res.*, 50 (2011), pp. 3798-3817.

D.W. Hutmacher, T. Schantz, I. Zein, K.W. Ng, S.H. Teoh and K.C. Tan **Mechanical properties and cell cultural response of polycaprolactone scaffolds designed and**

fabricated via fused deposition modeling. *J. Biomed. Mater. Res.*, 55 (2001), pp. 203-216.

S.E. Iismaa, X. Kaidonis, A.M. Nicks, N. Bogush, K. Kikuchi, N. Naqvi, R.P. Harvey, A. Husain and R.M. Graham **Comparative regenerative mechanisms across different mammalian tissues.** *NPJ Regen. Med.*, 3 (2018), pp. 6.

N. Jacquet, C.W. Lo, H.S. Wu, Y.H. Wei and S. Wang Shaw **Solubility of polyhydroxyalkanoates by experiment and thermodynamic correlations.** *AICHE Journal*, 53 (2007), pp. 2704-2714.

M. Janmohammadi and M.S. Nourbakhsh **Recent advances on 3D printing in hard and soft tissue engineering.** *Int. J. Polym. Mater. Polym. Biomater.*, (2019), pp. 1-18.

X. Jing, Z. Ling, Z. Zhenhu An, C. Guoqiang, G. Yandao, Z. Nanming and Z. Xiufang **Preparation and evaluation of porous poly(3-hydroxybutyrate-co-3-hydroxyhexanoate) hydroxyapatite composite scaffolds.** *J Biomater Appl*, 22 (2008), pp. 293-307.

V. Karageorgiou and D. Kaplan **Porosity of 3D biomaterial scaffolds and osteogenesis.** *Biomaterials*, 26 (2005), pp. 5474-5491.

S. Ke, Y. Yang, L. Ren, Y. Wang, Y. Li and H. Huang **Dielectric behaviors of PHBHHx–BaTiO₃ multifunctional composite films.** *Compos. Sci. Technol.*, 72 (2012), pp. 370-375.

Y. Ke, C. Liu, X. Zhang, M. Xiao and G. Wu **Surface Modification of Polyhydroxyalkanoates toward Enhancing Cell Compatibility and Antibacterial Activity.** *Macromol. Mater. Eng.*, 302 (2017), pp. 1700258.

M. Koller **Biodegradable and Biocompatible Polyhydroxy-alkanoates (PHA): Auspicious Microbial Macromolecules for Pharmaceutical and Therapeutic Applications.** *Molecules*, 23 (2018), pp. 362.

M. Koller, L. Maršálek, M.M. de Sousa Dias and G. Brauneegg **Producing microbial polyhydroxyalkanoate (PHA) biopolyesters in a sustainable manner.** *New Biotech.*, 37 (2017), pp. 24-38.

F.D. Kopinke, M. Remmler and K. Mackenzie **Thermal decomposition of biodegradable polyesters—I: Poly(β -hydroxybutyric acid).** *Polym. Degrad. Stab.*, 52 (1996), pp. 25-38.

W. Kosorn, M. Sakulsumbat, P. Uppanan, P. Kaewkong, S. Chantaweroad, J. Jitsaard, K. Sitthiseriratip and W. Janvikul **PCL/PHBV blended three dimensional scaffolds**

fabricated by fused deposition modeling and responses of chondrocytes to the scaffolds. *J. Biomed. Mater. Res. B Appl. Biomater.*, 105 (2016), pp. 1141-1150.

C. Kourmentza, J. Plácido, N. Venetsaneas, A. Burniol-Figols, C. Varrone, H.N. Gavala and M.A.M. Reis **Recent Advances and Challenges towards Sustainable Polyhydroxyalkanoate (PHA) Production.** *Bioengineering*, 4 (2017), pp. 55.

E. Leroy, I. Petit, J.L. Audic, G. Colomines and R. Deterre **Rheological characterization of a thermally unstable bioplastic in injection molding conditions.** *Polym. Degrad. Stab.*, 97 (2012), pp. 1915-1921.

S.-D. Li, J.-D. He, H. Yu Peter and K. Cheung Man **Thermal degradation of poly(3-hydroxybutyrate) and poly(3-hydroxybutyrate-co-3-hydroxyvalerate) as studied by TG, TG–FTIR, and Py–GC/MS.** *J. Appl. Polym. Sci.*, 89 (2003), pp. 1530-1536.

X.T. Li, Y. Zhang and G.Q. Chen **Nanofibrous polyhydroxyalkanoate matrices as cell growth supporting materials.** *Biomaterials*, 29 (2008), pp. 3720-3728.

S.C. Ligon, R. Liska, J. Stampfl, M. Gurr and R. Mülhaupt **Polymers for 3D Printing and Customized Additive Manufacturing.** *Chem. Rev.*, 117 (2017), pp. 10212-10290.

J.S. Lim, I. Noda and S.S. Im **Miscibility and crystallization behavior of poly(3-hydroxybutyrate-co-3-hydroxyhexanoate) and methoxy poly(ethylene glycol) blends.** *J. Polym. Sci., Part B: Polym. Phys.*, 44 (2006), pp. 2852-2863.

K.-Y. Lin, D.-M. Wang and J.-Y. Lai **Nonsolvent-Induced Gelation and Its Effect on Membrane Morphology.** *Macromolecules*, 35 (2002), pp. 6697-6706.

A. Morelli, D. Puppi and F. Chiellini **Polymers from Renewable Resources.** *J. Renew. Mat.*, 1 (2013), pp. 83-112.

C. Mota, D. Puppi, F. Chiellini and E. Chiellini **Additive manufacturing techniques for the production of tissue engineering constructs.** *J. Tissue Eng. Regen. Med.*, 9 (2015), pp. 174-190.

C. Mota, D. Puppi, D. Dinucci, M. Gazzarri and F. Chiellini **Additive manufacturing of star poly(ϵ -caprolactone) wet-spun scaffolds for bone tissue engineering applications.** *J. Bioact. Compat. Polym.*, 28 (2013), pp. 320-340.

C. Mota, S.Y. Wang, D. Puppi, M. Gazzarri, C. Migone, F. Chiellini, G.Q. Chen and E. Chiellini **Additive manufacturing of poly[(R)-3-hydroxybutyrate-co-(R)-3-hydroxyhexanoate] scaffolds for engineered bone development.** *J. Tissue Eng. Regen. Med.*, 11 (2017), pp. 175-186.

D. Puppi and F. Chiellini **Wet-spinning of biomedical polymers: from single-fibre production to additive manufacturing of three-dimensional scaffolds.** *Polym. Int.*, 66 (2017), pp. 1690–1696.

D. Puppi and F. Chiellini **Biofabrication via integrated additive manufacturing and electrofluidodynamics.** In *Electrofluidodynamic Technologies (EFDTs) for*

Biomaterials and Medical Devices. V. Guarino and L. Ambrosio, Woodhead Publishing. (2018): 71-85.

D. Puppi, F. Chiellini, M. Dash and E. Chiellini **Biodegradable Polymers for Biomedical Applications In Biodegradable Polymers: Processing, Degradation and Applications**. G.P. Felton, Nova Science Publishers, Inc. (2011): 545-604.

D. Puppi, C. Migone, L. Grassi, A. Piroso, G. Maisetta, G. Batoni and F. Chiellini **Integrated three-dimensional fiber/hydrogel biphasic scaffolds for periodontal bone tissue engineering**. *Polym. Int.*, 65 (2016a), pp. 631-640.

D. Puppi, A. Morelli, F. Bello, S. Valentini and F. Chiellini **Additive Manufacturing of Poly(methyl methacrylate) Biomedical Implants with Dual-scale Porosity** *Macromol. Mater. Eng.*, 303 (2018a), pp. 1800247.

D. Puppi, A. Morelli and F. Chiellini **Additive Manufacturing of Poly(3-hydroxybutyrate-co-3-hydroxyhexanoate)/poly(ϵ -caprolactone) Blend Scaffolds for Tissue Engineering**. *Bioengineering*, 4 (2017a), pp. 49.

D. Puppi, C. Mota, M. Gazzarri, D. Dinucci, A. Gloria, M. Myrzabekova, L. Ambrosio and F. Chiellini **Additive manufacturing of wet-spun polymeric scaffolds for bone tissue engineering**. *Biomed. Microdevices*, 14 (2012), pp. 1115-1127.

D. Puppi, A.M. Piras, A. Piroso, S. Sandreschi and F. Chiellini **Levofloxacin-loaded Star Poly(ϵ -caprolactone) Scaffolds by Additive Manufacturing**. *J. Mater. Sci. Mater. Med.*, 27 (2016b), pp. 44.

D. Puppi, A. Piroso, G. Lupi, P.A. Erba, G. Giachi and F. Chiellini **Design and fabrication of novel polymeric biodegradable stents for small caliber blood vessels by computer-aided wet-spinning**. *Biomed. Mater.*, 12 (2017b), pp. 035011.

D. Puppi, A. Piroso, A. Morelli and F. Chiellini **Design, fabrication and characterization of tailored poly[(R)-3-hydroxybutyrate-co-(R)-3-hydroxyhexanoate] scaffolds by computer-aided wet-spinning**. *Rapid Prototyp. J.*, 24 (2018b), pp. 1-8.

C. Romagnoli, R. Zonefrati, D. Puppi, C. Rosati, A. Aldinucci, G. Palmi, G. Galli, F. Chiellini, F.S. Martelli, A. Tanini and M.L. Brandi **Human Adipose Tissue-Derived Stem Cells and a Poly(ϵ -Caprolactone) Scaffold Produced by Computer-Aided Wet Spinning for Bone Tissue Engineering**. *J. Biomater. Tissue Eng.*, 7 (2017), pp. 622-633.

S. Saska, L.C. Pires, M.A. Cominotte, L.S. Mendes, M.F. de Oliveira, I.A. Maia, J.V.L. da Silva, S.J.L. Ribeiro and J.A. Cirelli **Three-dimensional printing and in vitro evaluation of poly(3-hydroxybutyrate) scaffolds functionalized with osteogenic growth peptide for tissue engineering**. *Mater. Sci. Eng., C*, 89 (2018), pp. 265-273.

H. Sato, M. Nakamura, A. Padermshoke, H. Yamaguchi, H. Terauchi, S. Ekgasit, I. Noda and Y. Ozaki **Thermal Behavior and Molecular Interaction of Poly(3-**

hydroxybutyrate-co-3-hydroxyhexanoate) Studied by Wide-Angle X-ray Diffraction. *Macromolecules*, 37 (2004), pp. 3763-3769.

M.R. Sommer, M. Schaffner, D. Carnelli and A.R. Studart **3D Printing of Hierarchical Silk Fibroin Structures.** *ACS Appl. Mater. Interfaces*, 8 (2016), pp. 34677-34685.

D. Wang, K. Li and W.K. Teo **Relationship between mass ratio of nonsolvent-additive to solvent in membrane casting solution and its coagulation value.** *J. Membr. Sci.*, 98 (1995), pp. 233-240.

D. Wang, W.K. Teo and K. Li **Preparation and characterization of high-flux polysulfone hollow fibre gas separation membranes.** *J. Membr. Sci.*, 204 (2002), pp. 247-256.

Y. Wang, Y.-Z. Bian, Q. Wu and G.-Q. Chen **Evaluation of three-dimensional scaffolds prepared from poly(3-hydroxybutyrate-co-3-hydroxyhexanoate) for growth of allogeneic chondrocytes for cartilage repair in rabbits.** *Biomaterials*, 29 (2008), pp. 2858-2868.

Y. Wang and G.-Q. Chen **Polyhydroxyalkanoates: Sustainability, Production, and Industrialization.** In *Sustainable Polymers from Biomass*. C. Tang and C.Y. Ryu, Wiley-VCH Verlag GmbH & Co. KGaA. (2017): 11-33.

Y. Wang, R. Gao, P.-P. Wang, J. Jian, X.-L. Jiang, C. Yan, X. Lin, L. Wu, G.-Q. Chen and Q. Wu **The differential effects of aligned electrospun PHBHHx fibers on adipogenic and osteogenic potential of MSCs through the regulation of PPAR γ signaling.** *Biomaterials*, 33 (2012), pp. 485-493.

Y. Wang, X.-L. Jiang, S.-C. Yang, X. Lin, Y. He, C. Yan, L. Wu, G.-Q. Chen, Z.-Y. Wang and Q. Wu **MicroRNAs in the regulation of interfacial behaviors of MSCs cultured on microgrooved surface pattern.** *Biomaterials*, 32 (2011), pp. 9207-9217.

Y.W. Wang, Q. Wu and G.Q. Chen **Attachment, proliferation and differentiation of osteoblasts on random biopolyester poly(3-hydroxybutyrate-co-3-hydroxyhexanoate) scaffolds.** *Biomaterials*, 25 (2004), pp. 669-675.

Y.W. Wang, F. Yang, Q. Wu, Y.C. Cheng, P.H. Yu, J. Chen and G.Q. Chen **Effect of composition of poly(3-hydroxybutyrate-co-3-hydroxyhexanoate) on growth of fibroblast and osteoblast.** *Biomaterials*, 26 (2005), pp. 755-761.

W.R. Webb, T.P. Dale, A.J. Lomas, G. Zeng, I. Wimpenny, A.J. El Haj, N.R. Forsyth and G.-Q. Chen **The application of poly(3-hydroxybutyrate-co-3-hydroxyhexanoate) scaffolds for tendon repair in the rat model.** *Biomaterials*, 34 (2013), pp. 6683-6694.

J.G. Wijmans and C.A. Smolders **Preparation of Asymmetric Membranes by the Phase Inversion Process.** In *Synthetic Membranes: Science, Engineering and Applications*. P.M. Bungay, Lonsdale, H.K., de Pinho, M.N. Dordrecht, Holland, Springer Netherlands. (1982): 39-56.

L.-P. Wu, M. You, D. Wang, G. Peng, Z. Wang and G.-Q. Chen **Fabrication of carbon nanotube (CNT)/poly(3-hydroxybutyrate-co-3-hydroxyhexanoate)**

(PHBHHx) nanocomposite films for human mesenchymal stem cell (hMSC) differentiation. Polym. Chem., 4 (2013), pp. 4490-4498

H. Xiang, X. Wen, X. Miu, Y. Li, Z. Zhou and M. Zhu **Thermal depolymerization mechanisms of poly(3-hydroxybutyrate-co-3-hydroxyvalerate).** Pro. Nat. Sci.-Mater., 26 (2016), pp. 58-64.

H.-X. Yang, M. Sun and P. Zhou **Investigation of water diffusion in poly(3-hydroxybutyrate-co-3-hydroxyhexanoate) by generalized two-dimensional correlation ATR-FTIR spectroscopy.** Polymer, 50 (2009), pp. 1533-1540.

M. Yang, S. Zhu, Y. Chen, Z. Chang, G. Chen, Y. Gong, N. Zhao and X. Zhang **Studies on bone marrow stromal cells affinity of poly (3-hydroxybutyrate-co-3-hydroxyhexanoate).** Biomaterials, 25 (2004), pp. 1365-1373.

A. Youssef, S.J. Hollister and P.D. Dalton **Additive manufacturing of polymer melts for implantable medical devices and scaffolds.** Biofabrication, 9 (2017), pp. 012002.

K. Zhang, Y. Fan, N. Dunne and X. Li **Effect of microporosity on scaffolds for bone tissue engineering.** Regen. Biomater., 5 (2018), pp. 115-124.

Tables

Table 1. Ternary PHBHHx/chloroform/ethanol mixtures.

Mixture	Mixing method	Solvent/non-solvent (% v/v)	Solubility*	Scaffold fabrication
M-100S	–	100	a	✓
M1-90S-10NS	M1	90:10	a	✓
M2-90S-10NS	M2	90:10	a	✓
M1-80S-20NS	M1	80:20	a	✓
M2-80S-20NS	M2	80:20	a	✓
M1-70S-30NS	M1	70:30	a	✓
M2-70S-30NS	M2	70:30	a	✓
M1-60S-40NS	M1	60:40	b	✓
M2-60S-40NS	M2	60:40	b	✓
M1-50S-50NS	M1	50:50	c	✗
M2-50S-50NS	M2	50:50	c	✗

M1: Mixture method 1; M2: Mixture method 2; S: Solvent (chloroform); NS: Non-solvent (ethanol); *solubility assessed at a concentration of 25% w/v; a: soluble, b: partially soluble, c: poorly soluble.

Table 2. Scaffolds thermal properties from TGA and DSC analysis.

Sample	Tdeg (°C)	Tg I (°C)	Tg II (°C)	Tm (°C)	Cr (%)
PHBHHx raw	227.2 ± 2.1 ⁺	-0.4 ± 0.4	-0.4 ± 0.3	87.9 ± 0.5 ⁺	18.4 ± 1.7 ⁺
M-100S	249.6 ± 3.1	-0.6 ± 0.6	-0.4 ± 0.4	95.0 ± 0.2	21.4 ± 1.6
M1-90S-10NS	242.2 ± 0.2	-1.3 ± 0.5	-0.6 ± 0.6	95.2 ± 0.4	22.6 ± 0.7
M2-90S-10NS	241.8 ± 1.9	-0.6 ± 0.4	-0.6 ± 0.5	95.0 ± 0.6	23.0 ± 0.5
M1-80S-20NS	241.6 ± 1.4	-0.9 ± 0.5	-0.4 ± 0.4	94.9 ± 0.2	23.3 ± 0.2
M2-80S-20NS	243.0 ± 3.9	-0.5 ± 0.4	-0.9 ± 0.8	94.6 ± 0.7	22.0 ± 1.2
M1-70S-30NS	243.5 ± 0.3	-0.5 ± 0.4	-0.7 ± 0.6	95.0 ± 0.1	22.0 ± 1.5
M2-70S-30NS	242.1 ± 0.2	-0.9 ± 1.3	-1.2 ± 1.0	94.5 ± 0.3	22.2 ± 0.6
M1-60S-40NS	243.3 ± 0.2	-1.1 ± 1.1	-0.2 ± 0.2	94.5 ± 0.2	21.5 ± 1.5
M2-60S-40NS	240.0 ± 1.1	-1.0 ± 0.6	-0.4 ± 0.5	94.2 ± 0.4	22.5 ± 0.2

T_{deg}: degradation temperature; T_g: glass transition temperature acquired from first (I) or second (II) heating cycle; T_m: melting temperature; Cr: crystalline percentage degree.

⁺Value significantly lower when compared to those of the other scaffolds (p<0.05).

Figure captions

Figure 1. Scaffold design and manufacturing by CAWS: schematic representation of (a) fabrication apparatus and (b) designed scaffold structural parameters. (d_{XY} : distance between deposition lines; d_z : interlayer needle translation along Z axis; α : lay-down pattern angle).

Figure 2. PHBHHx scaffolds fabrication by CAWS: representative pictures of samples fabricated by processing polymeric solutions with different solvent/non-solvent ratio (16 layers, measure unit: 1 mm).

Figure 3. Thermal characterization of PHBHHx samples: representative (a) TGA derivative weight curves and (b) DSC 1st heating thermograms.

Figure 4. Morphological characterization of PHBHHx scaffolds (16 layers): representative SEM micrographs taken from top view (600x, scale bar: 200 μm) or perpendicular cross-section (200x, scale bar: 500 μm).

Figure 5. High magnification morphological analysis of PHBHHx scaffolds: representative SEM micrographs of (a) perpendicular cross-section of scaffolds with different Z axis inter-fiber distance (800x, scale bar: 100 μm); (b) fiber cross-section (3000x, scale bar: 40 μm) and fiber external surface (2000x, scale bar: 50 μm) of scaffolds with different micropores concentration.

Figure 6. Statistical analysis of macro-and micromorphological parameters of PHBHHx scaffolds: (a) fiber diameter, (b) macropores size along Z axis, (c) micropores concentration, (d) overall porosity. Data expressed as mean \pm standard deviation.

+ For a given parameter, value significantly different when compared to the others ($p < 0.05$).

*** For a given parameter, values marked with the same number of * are not significantly different when compared between them, but significantly different when compared with the other values ($p < 0.05$).

°• For a given parameter, values marked with the same number of ° or • are significantly different when compared between them ($p < 0.05$).

Figure 7. Mechanical characterization of PHBHHx scaffolds under a constant tensile strain ($3.5 \text{ mm} \cdot \text{min}^{-1}$) parallel to longitudinal fibers axes: (a) representative stress-strain curves, (b) tensile modulus, (c) stress at break. Data expressed as mean \pm standard deviation ($n=5$).

+ Value significantly different when compared to the others ($p < 0.05$)

* Values significantly different when compared with the other values but not between them ($p < 0.05$).

Figure 8. MC3T3-E1 cell proliferation on PHBHHx scaffolds. Data expressed as mean \pm standard deviation.

* For a given parameter, values are not significantly different when compared between them ($p < 0.05$).

Figure 9. CLSM microphotographs showing MC3T3-E1 cell cultured on PHBHHx based scaffolds at day 16 of culture (magnification 10X and 20X).

Figure 1

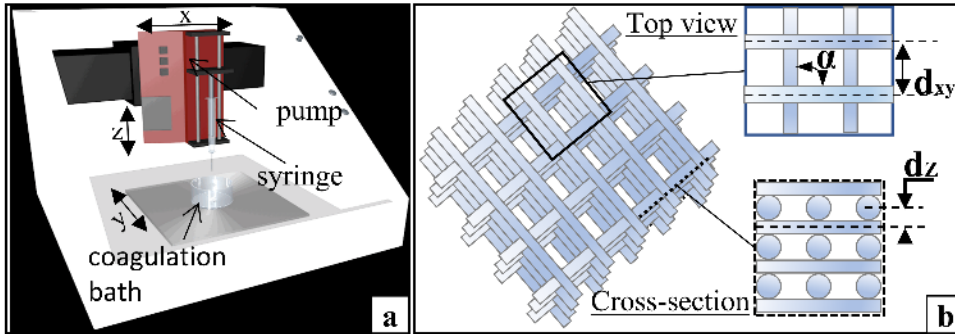


Figure 2

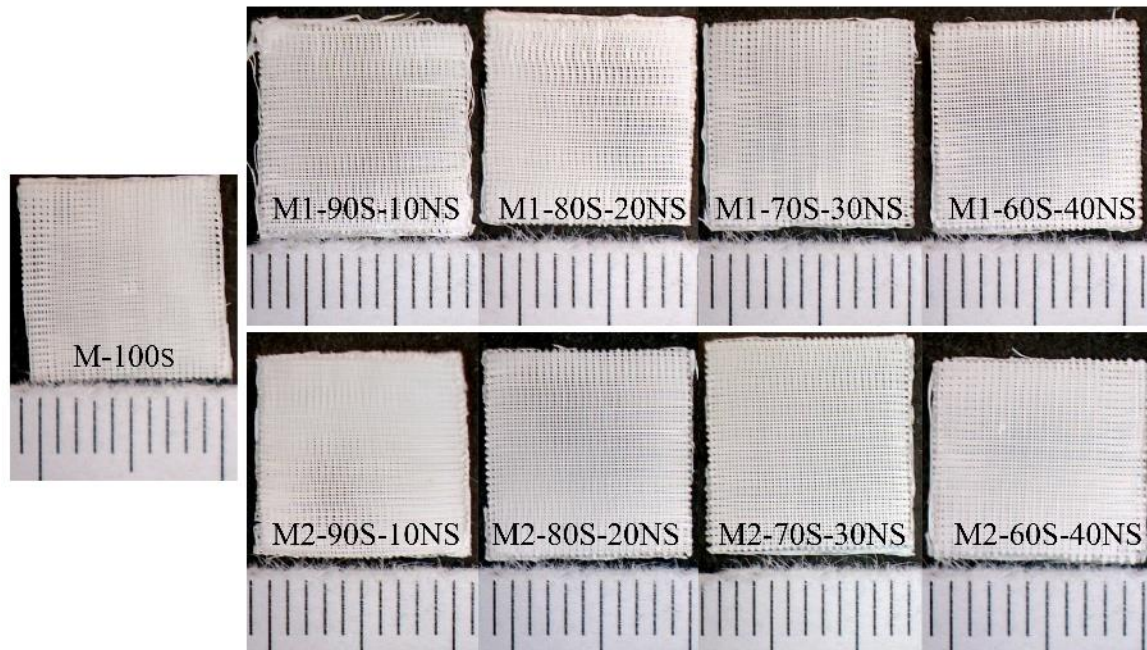


Figure 3

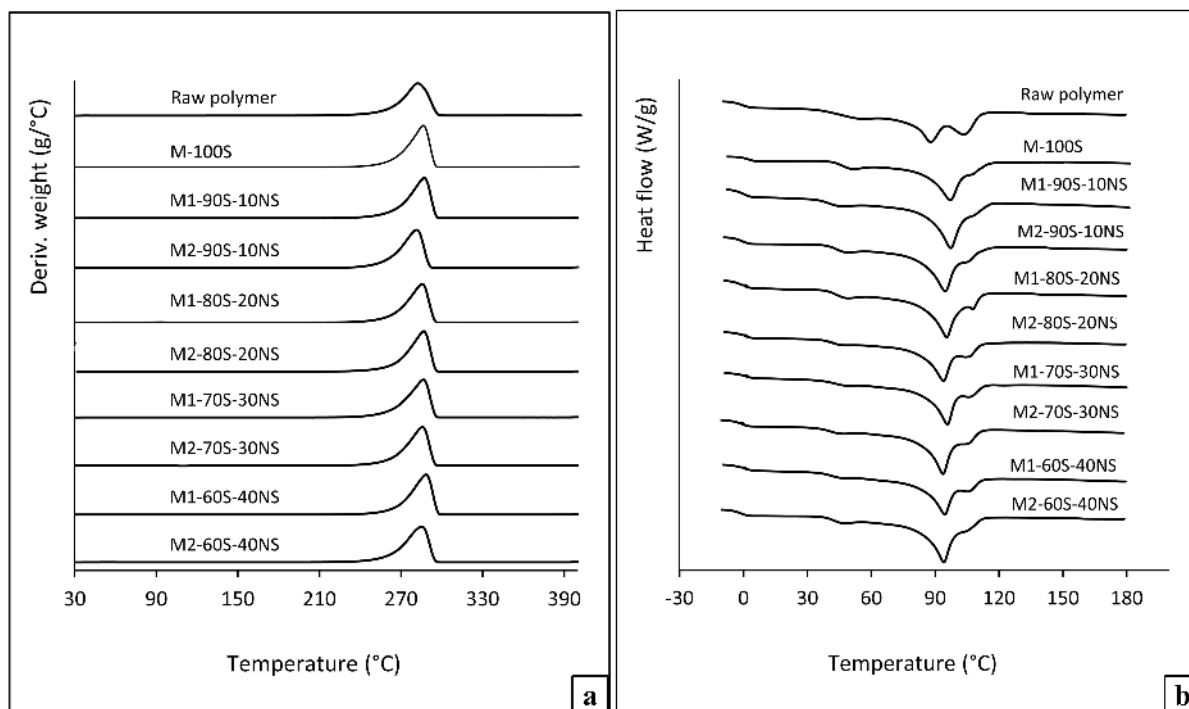


Figure 4

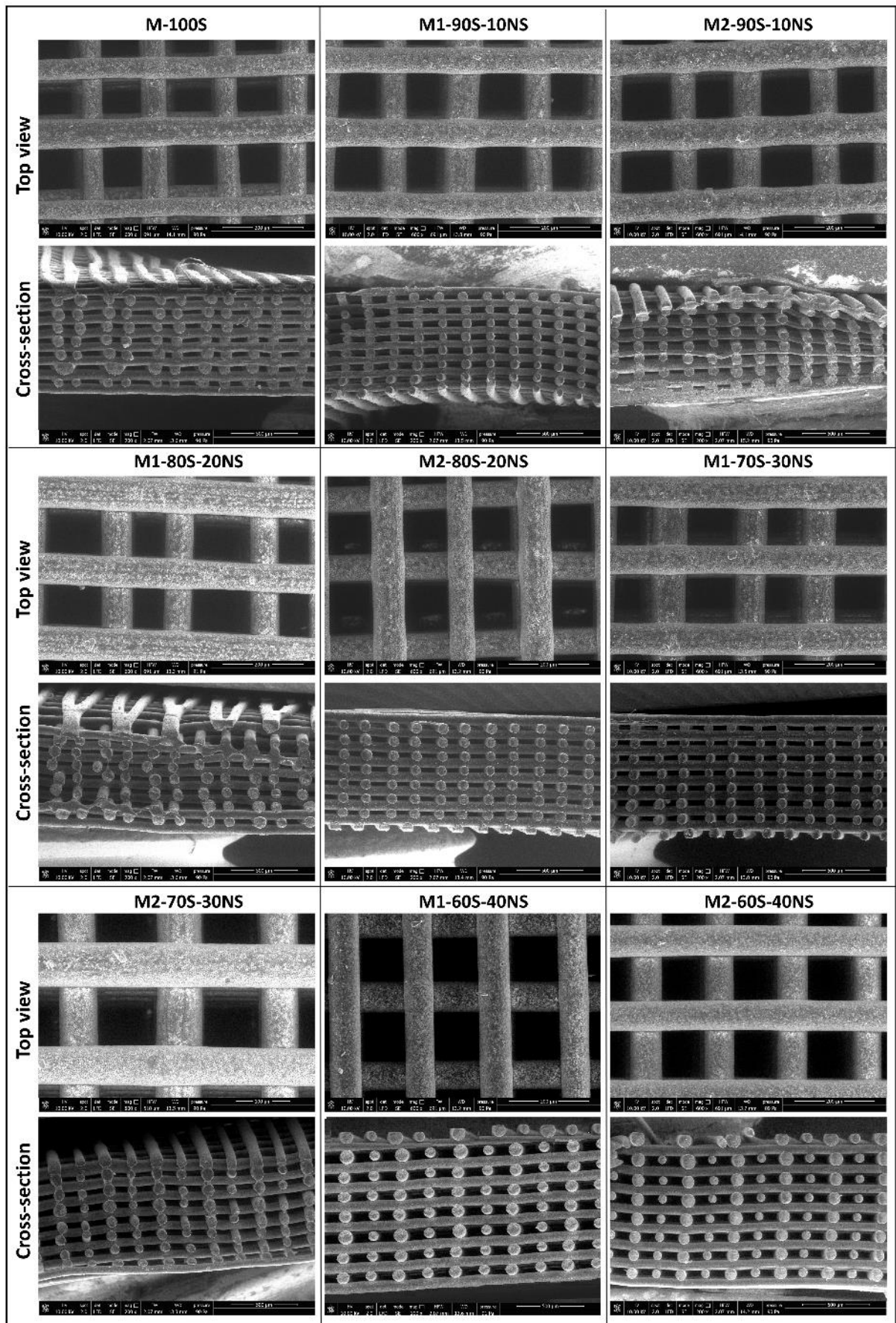


Figure 5

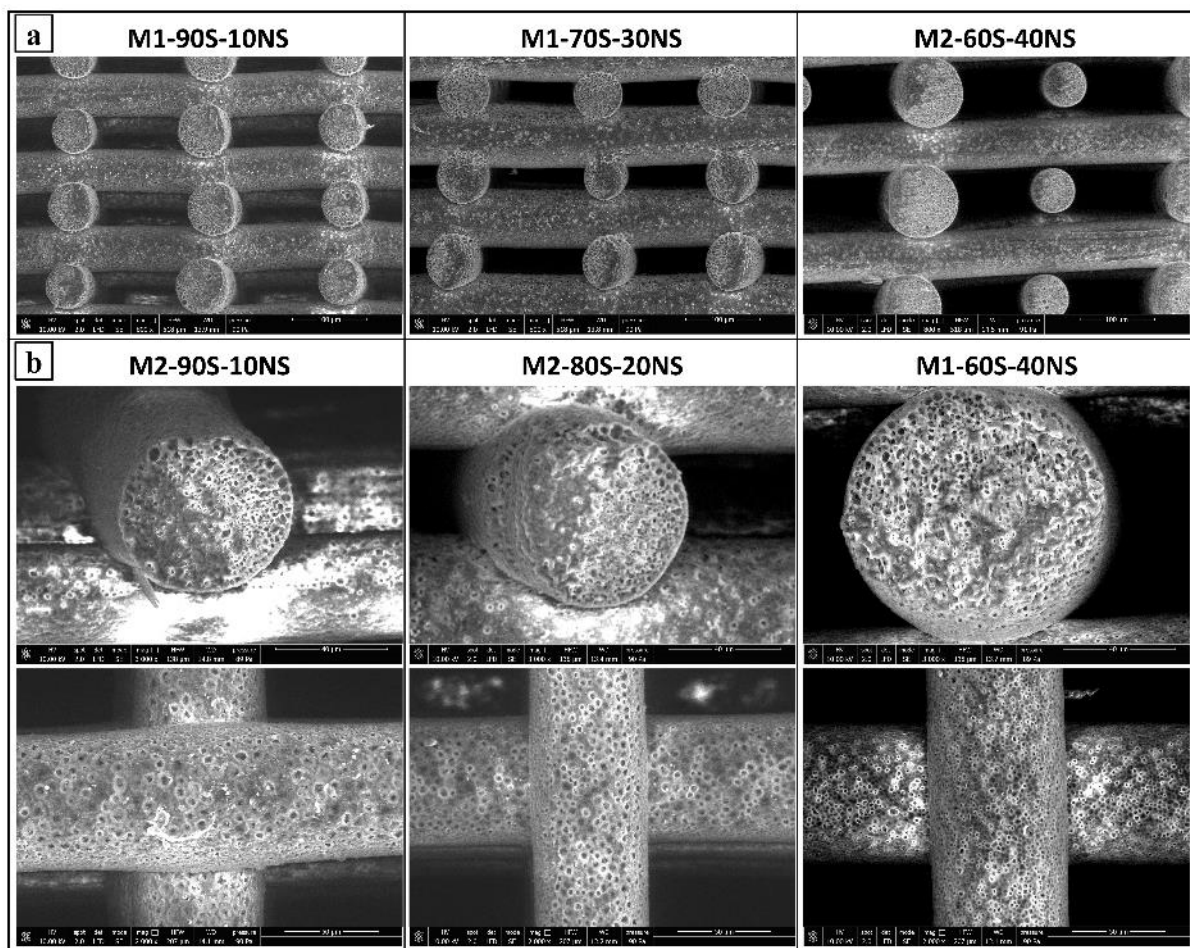


Figure 6

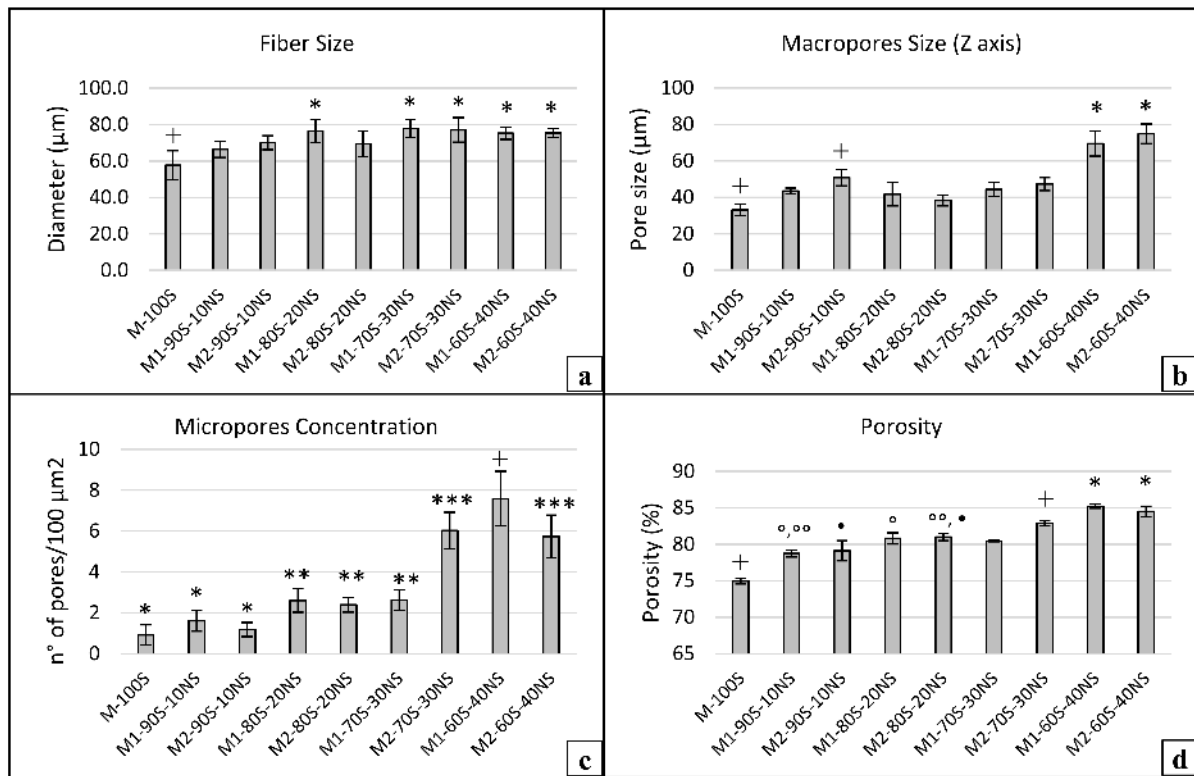


Figure 7

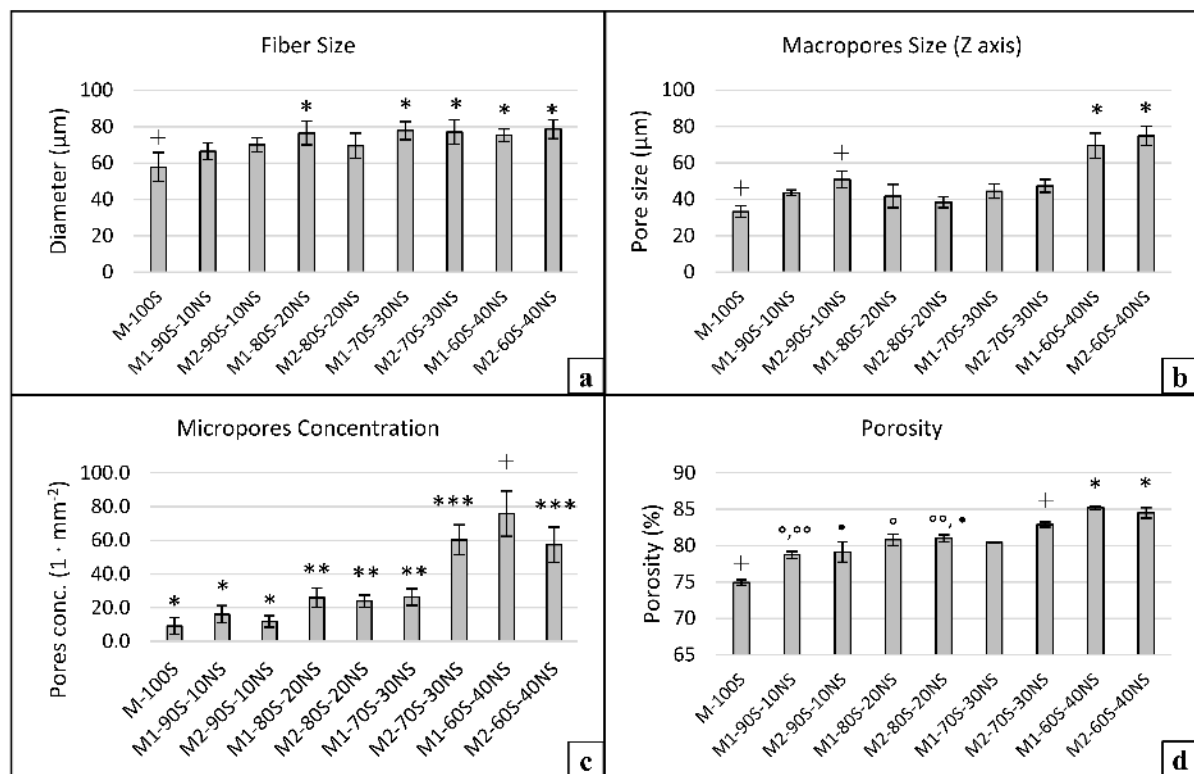


Figure 8

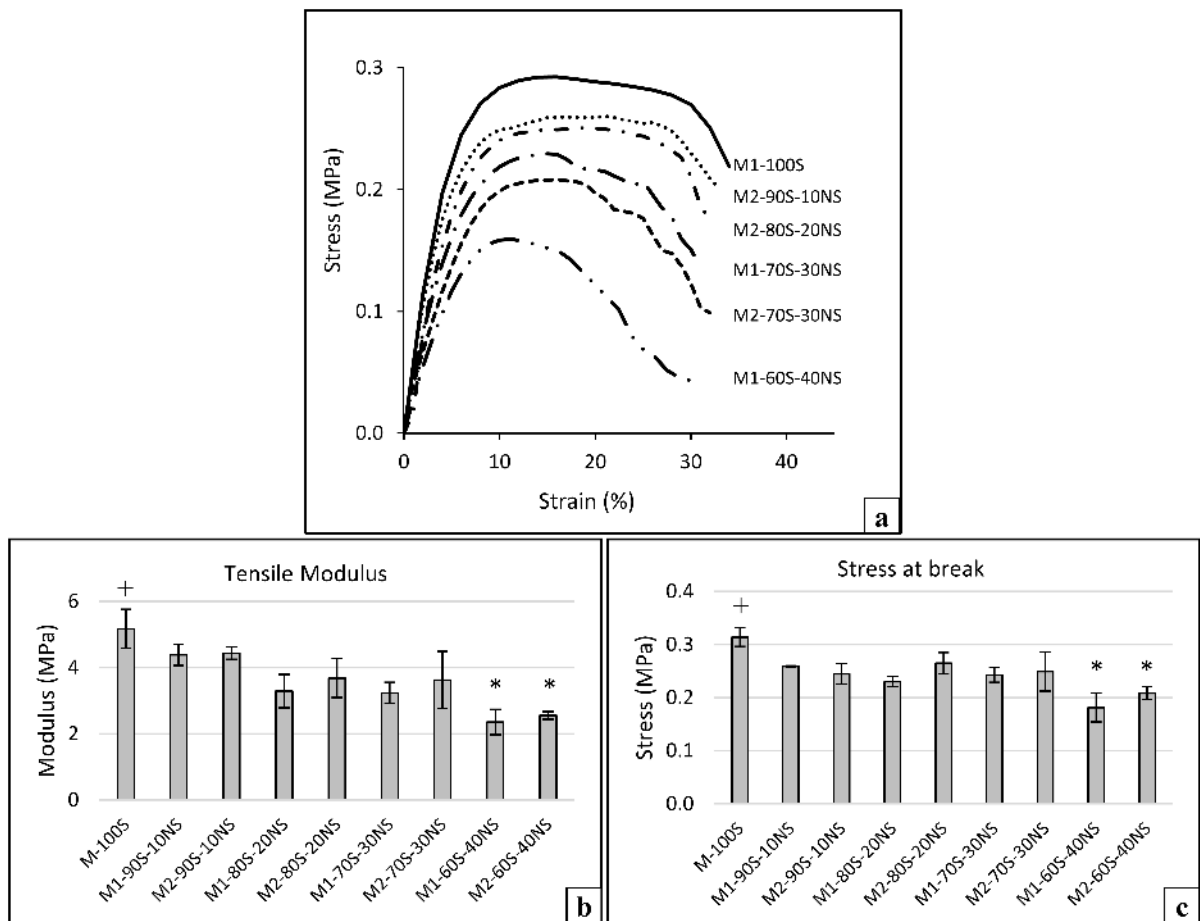


Figure 9

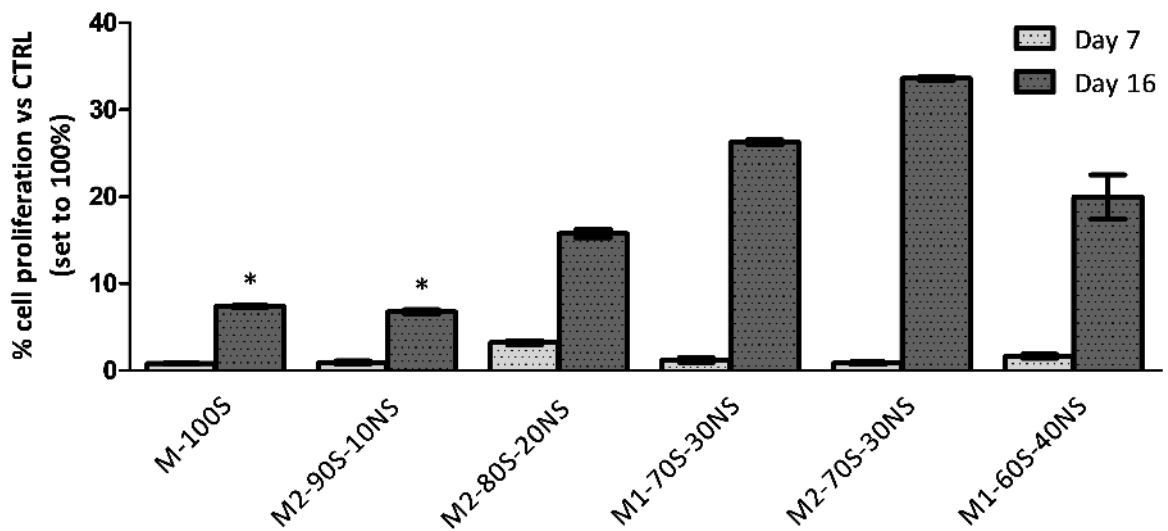


Figure 10

